District-Scale Resilient System Design

Antoine Gautier[a], Michael Wetter[a,*], Matthias Sulzer[b]

[a]*Lawrence Berkeley National Laboratory, Berkeley, CA, USA*
[b]*Empa, Dübendorf, Switzerland*

Abstract

Keywords: District Heating and Cooling, Modelica, Modeling and Simulation, Resilience, Numerical Performance

1. Abstract

Novel district heating and cooling systems allow sharing large geothermal resources between buildings by operating a central water loop near ground temperature, coupled to distributed vapor-compression machines that lift the temperature up or down to what the building's heating or cooling system requires. Originally designed to capture heat from low-temperature heat sources more efficiently, those systems also provide opportunities for compressor-less cooling.

Using high-fidelity models of buildings, district energy, building-side HVAC and control systems, we are assessing how to improve resilience of buildings during heat waves and power outages, during which we switch the system from normal operation to a resilience mode at low power.

The sensitivity of the overall system performance in the resilience mode is investigated with regards to the configuration of the primary systems (integration of a waterside economizer, auxiliary cooling), the sizing parameters (cooling coils, fans, geothermal borefield) and the control principles. Furthermore, the positive externality of a design optimized for resilience is evaluated under standard operating conditions to illustrate to what extent the increased first cost at the building level is balanced by a lower average heat rejection from the compressors that yields sizing margins of the central systems, or how the design for low-power resilient conditioning also contributes to reducing the HVAC energy demand over the year at the district scale.

2. Introduction

The system under investigation is a district heating and cooling (DHC) system for cold networks[1] with distributed heat recovery chillers. The main network distributes water near ground

*Corresponding author.

[1]Although the terminology of fifth generation DHC has been widely used to refer to those systems (Buffa et al., 2019), it is disputed in (Sulzer et al., 2021) which advocates for a distinction in terms of configuration rather than generation, the configuration being called combined heating and cooling for use in cold networks, the generation remaining the fourth. Referring to a specific hydronic arrangement for that kind of system, Sommer et al. (2020) introduces the concept of reservoir network, which makes explicit another distinguishing feature, that is the low-temperature source that these networks allow connecting to—either waste heat from process applications, or environmental heat from geothermal plants, ground water and lakes. A similar terminology is used in France where the concept of ambient loop based on geothermal energy is used (AFPG, 2020).

temperature, typically between 9°C and 16°C. A large central geothermal borefield is used for seasonal heat storage while auxiliary coolers cater for the annual load imbalance where the heat rejection demand often dominates in mixed-use applications.

Buffa et al. (2019) shows a growing trend in the adoption of such novel DHC systems, with about 40 systems in operation in Europe as of 2018. Additionally, AFPG (2020) inventories 16 systems in France as of 2020.

The potential benefits of such design are indeed numerous. The compressor lift is optimized on both sides. On the load side, the supply temperature is driven by the reset logic of each building HVAC system, as opposed to the limiting set point among all connected buildings in case of a central plant. On the source side, the heat rejected by cooling dominated buildings contributes to increasing the loop temperature level, which is beneficial to heating dominated buildings, and vice versa. Heat recovery is possible over the whole network, not only between buildings as described before, but because of the ultra-low temperature network, virtually with any source of low-quality heat, such as condenser water used from process cooling or even sewage water as low as 15°C. Compressor-less cooling is achievable at a temperature level compatible with radiant cooling systems. The resilience of the connected buildings is improved in case of heat waves, as well chiller failure. The low temperature in the main network allows using uninsulated pipes made of polymeric materials, reducing first costs and potentially increasing the heat storage capacity through the thermal coupling with the ground.

Among the main drawbacks, the following may be mentioned. The design and operation of the energy transfer stations is more critical, and strongly impacted by the network topology (Wetter and Hu, 2019b). For instance, hydronic unbalances are likely to yield a chiller trip out of high condenser pressure. The maintenance costs may increase due to the distributed architecture, although servicing small screw chillers typically requires less specialized skills than large capacity chillers in central plants.

Several articles (Wetter and Hu, 2019b), (Sommer et al., 2020) investigate the efficiency of those systems in configurations where the aggregated load profile is heating dominated and heat is harvested on a low temperature source. However, no articles could be found that explore the compressor-less cooling capabilities—which are often presented as a distinguishing feature of those systems—in cooling dominated load profiles—which are the most common cases in mixed-use developments or campus applications. We propose to address that matter and understand its implications on the main components of the system, in terms of equipment type, hydronic layout, controls and sizing.

We also propose a focus on the design principles of the energy transfer station (ETS). Indeed, with distributed architectures, the ETS becomes one of the critical components of the system. However, only a couple articles (Buffa et al., 2020), (Wetter and Hu, 2019b) address the corresponding design challenges, and none of them provides insight on a compressor-less cooling mode.

Regarding the design of the geothermal system, our goal is to illustrate to what extent conventional sizing methods used for ground-source heat pump systems (Kavanaugh and Rafferty, 2014) can inform the design of a large-scale, hybrid and distributed system, where those methods fall short, and where a model-based design becomes necessary for equipment selection and sizing.

Eventually, to help inform the design of a resilient urban energy infrastructure, we propose to investigate how the technology can be integrated with existing all-air systems, which are by far the most widely used in the US and the least favorable for high-temperature cooling (as opposed to radiant cooling systems). We thus aim to question how novel DHC technologies can be deployed

to existing buildings and if compressor-less cooling opportunities are accessible to typical air-based systems.

The rest of this paper is organized as follows. - Modeling Framework - System Characteristics and Operating Principles - Simulation Experiment - Results and Discussion

3. Modeling Framework

All the numerical models used in this analysis are developed with the Modelica language (Mattsson and Elmqvist, 1997). The large majority of them are distributed within the Modelica Buildings Library (MBL) version 8.0.0, an open-source model library that is based on the Modelica IBPSA Library (Wetter et al., 2015) developed in IBPSA Project 1 (Wetter et al., 2019). The use of that modeling framework can be readily motivated when enumerating the variables of interest for our analysis, namely the chiller, pump and fan power, that all depend strongly on the control principles such as resetting the chilled water (CHW) supply temperature or the duct static pressure, modulating the pump speed, with feedback from on a remote differential pressure sensor, or a control valve position, etc. Two built-in features of the MBL appear critical for that kind of system analysis: the ability to model controls in a physically realistic and efficient way, and the pressure-driven fluid flow modeling.

In addition, for the purpose of the indoor comfort analysis, we need access to a building room model that can be easily parameterized and coupled to a detailed HVAC system model, and that enables computing both the air and the indoor surfaces temperature.

The MBL comes with the Spawn of EnergyPlus components (Wetter et al., 2020) that support seamless coupling of EnergyPlus envelope and access to prototypical buildings and standard load profiles

Flexible framework with replaceable components that allow switching easily the building load models and testing system and control variants.

Reference URBANopt paper

4. Description of the Main Components of the DHC System

4.1. Energy Transfer Station

The concept behind the energy transfer station (ETS) was first investigated on a mixed-use development project with distributed geothermal borefields (Wetter and Hu, 2019a). It relies on heat recovery chillers[2] and a load balancing control logic that uses the ambient source—such as the service water through the interface heat exchanger—to drop the excess heat or the excess cold depending on the current operating conditions.

[2]Heat recovery chillers are typically built with scroll or screw compressors that are capable of operating at a high condenser leaving temperature (the operating limit observed across various manufacturers lies around 63°C). That makes that equipment suitable for both heating hot water and domestic hot water production. The drawback is that the compressor is operated at a high lift which is detrimental to the efficiency. A potentially more efficient design is proposed in Cline and Bakkum (2020) where at least two separate units are used and the source-side circuits are connected together with the ambient source (a geothermal borefield in that case), resulting in cascading thermodynamic cycles when the plant operates in simultaneous heating and cooling mode.

The system schematic is presented Figure 1, which also includes the design conditions considered for sizing the different components. We will now summarize the main operating principles. For further details, the reader may refer to the documentation of the model `Buildings.Experimental.DHC.EnergyTransferStations.Combined.Generation5.ChillerBorefield` distributed within the Modelica Buildings Library (from the commit `4a6285f`).

- The supervisory controller ensures the load balancing between the condenser side and the evaporator side of the chiller.

  The temperature at the top of the hot water buffer tank is controlled within a dead band above the supply temperature set point. When the temperature reaches the lower limit, cold rejection is activated to create a false load on the evaporator and thus increase the heat transfer rate at the condenser. When the temperature reaches the upper limit, heat rejection is activated.

  The maximum signal between heat and cold rejection u_{Rej} is used to control in sequence the optional geothermal borefield (priority system), the district heat exchanger (second priority system), and ultimately the chiller, by resetting down the CHW supply temperature.

  In addition, a controller is used to track the chilled water supply temperature set point at the bottom of the chilled water buffer tank. This controller acts against the ambient source control signal to limit the cold rejection when the set point is not met. This is needed because of the parallel arrangement of the evaporator loop and the ambient loop, where the latter can "steal" primary flow rate that will not reach the buffer tank, which can lead to secondary flow recirculation. This will increase the temperature at the bottom of the tank and creates a demand that will limit the flow rate in the ambient loop. Note that secondary flow recirculation may still happen if the chiller set point (as set by the supervisory controller) is lower than the chilled water supply temperature set point (as set by the building automation system).

  This control logic based on opposing PI controllers was preferred to a discrete logic based on a set of operating modes, where cycling between the different modes was difficult to avoid.

  The only remaining discrete control logic pertains to the actuation of the isolation valves between the condenser and evaporator loops and the ambient loops. Here a simple logic based on the return position of the opposite valve and a non zero heat or cold rejection demand is implemented to open the valve (with additional timers to avoid short cycling).

- The district heat exchanger realizes the interface between the building system and the district system. It is controlled with the heat or cold rejection signal u_{Rej} yielded by the supervisory controller. The primary and secondary circuits are enabled to operate if u_{Rej} is greater than zero and at least one isolation valve is proven open. When enabled, the secondary circuit is controlled based on u_{Rej}, which is mapped to modulate in sequence the mixing valve and the pump speed. (The mixing valve is needed to stabilize the control of the system when the secondary mass flow rate required to meet the heat or cold rejection demand is below the minimum flow rate to operate the pump.) The primary pump speed (or valve opening) is directly modulated with u_{Rej}.

  This was preferred to a control based on the temperature due to the variation of the temperature difference between the secondary and primary side when switching between heat

rejection (with large temperature difference) and cold rejection (with small temperature difference, as used for sizing). This required gain scheduling and turned out difficult to tune. However, the simpler logic based on the heat or cold rejection demand brings additional requirements regarding hydronic balancing, see §Appendix A.

- The optional waterside economizer (WSE) is enabled if there is a cooling demand, and the evaporator isolation valve is closed (i.e., the system is not in cold rejection mode), and the predicted leaving water temperature is lower than the entering water temperature (with additional timers to avoid short cycling). The system is disabled if any of the previous conditions is not met, except that the actual leaving water temperature is used instead of the predicted value. When the system is enabled the bypass valve on the secondary side is fully closed and the primary side is controlled so that the primary flow rate varies linearly with the secondary flow rate.

  The waterside economizer is integrated sidestream (on the secondary side) where the CHW temperature is the warmest to maximize the rate of heat transfer at given mass flow rates. However, it is not integrated into the condenser loop because the economizer operates mainly in the shoulder or cold season (with lower cooling loads allowing CHW supply temperature reset and lower service water temperature) when heating loads require a high condenser temperature (higher than the CHW return temperature).

- The condenser and evaporator pumps are enabled if there is a cooling or a heating demand (see §4.2). When enabled, the pumps are operated at constant speed, and the condenser (resp. evaporator) mixing valve is modulated with a PI loop controlling the minimum (resp. maximum) inlet temperature. The chiller is enabled when the pumps are proven on. It is controlled based on the chilled water supply temperature set point yielded by the supervisory controller.

4.2. Demand Signal, Supply Temperature Reset and Secondary Pump Control

The heating and cooling demand signals are computed based on the maximum control signals of the terminal units: whenever a terminal controller yields a non-zero signal (considering a small hysteresis) the demand signal switches to true.

If there is no demand, the secondary pump is disabled, and the supply temperature is reset to the least extreme value, allowing to operate the chiller at low lift.

If there is a demand, the secondary pump is enabled and its speed is modulated with a PI controller tracking a differential pressure set point at the most remote unit[3], and the supply temperature is reset with a PI controller tracking the maximum opening of the control valves of the terminal units to match 90%. We noticed that it is important to reset the controller output so that the design set point value is used when the demand signal switches to true. Otherwise there is a significant delay in satisfying the load, followed by a large overshoot, and the control loop is particularly hard to tune.

[3]Modern control sequences Taylor Engineering LLP et al. (2019) use a cascade control and reset in sequence the differential pressure set point of the distribution pump (up, first) and the CHW supply temperature set point (down, last) when the number of requests yielded by the terminal units increases—giving the priority to maintaining a low compressor lift over a low pump speed—although this sequenced control is shown to be only slightly better than resetting CHW supply temperature alone.

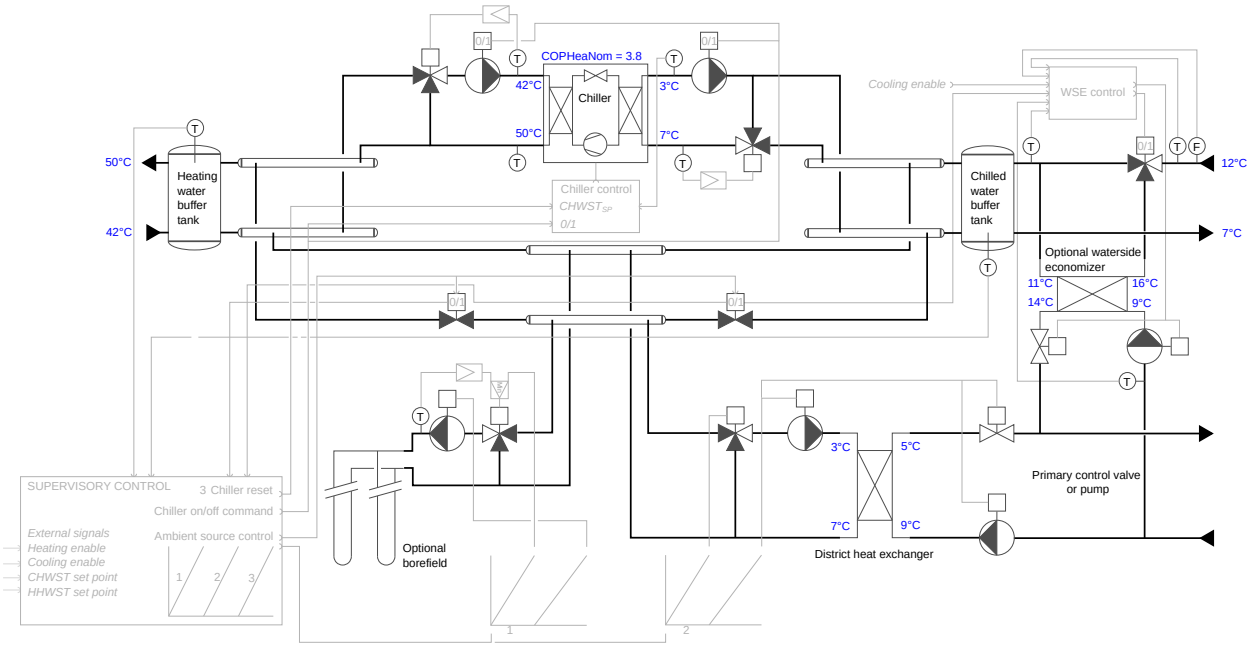

Figure 1: Schematic of the energy transfer station.

4.3. Central Systems

4.3.1. Loop Temperature Range

The target range for the supply temperature in the main loop is set at $[9, 16]$°C given the constraints on

- the minimum temperature of the fluid leaving the evaporator, which is typically around 3°C for water without glycol, and the chilled water delta-T, which is set at 4 K for both the primary and secondary circuits,
- the maximum CHW supply temperature in WSE mode compatible with radiant cooling, which is set at 18°C,
- the heat exchanger approach, which is taken equal to 2 K at design conditions for both the district heat exchanger and the waterside economizer.

4.3.2. Hydronic Network

Uninsulated HDPE pipes are considered, with an hydraulic diameter computed based on a design pressure drop of 250 Pa/m. A pipe length of 200 m is considered between each building, as well as a 50 m long service line.

The main distribution pump is sized considering no load diversity as the actual diversity observed on the load data (see §5.1.1) is close to 100%. The speed of the main distribution pump is modulated with a PI controller tracking a constant pressure differential set point at a remote location. A bypass line is modeled and is sized to recirculate 5% of the design flow rate at the pressure differential set point.

4.3.3. Geothermal Borefield

In this paragraph we describe the main characteristics of the ground heat exchanger while providing a first assessment of the number of boreholes based on a conventional sizing method, for both the heating and cooling requirements. The simulation study will then explore the sizing range in-between those two numbers. The main question we shall answer is to what extent the size of the borefield can be reduced—adopting a hybrid system design—while still providing enough capacity to maintain the loop supply temperature under an acceptable limit during an extreme week.

Kavanaugh and Rafferty (2014) propose a sizing method where the total borehole length L (m) is given by Equation 1.

$$L = \frac{\dot{Q}_a R_{10y} + \dot{Q}_m R_{1m} + \dot{Q}_h \left(R_b + F_{sc} R_{6h}\right)}{\left(T_{Ent} + T_{Lvg}\right)/2 - \left(T_g + T_p\right)} \tag{1}$$

with

$\dot{Q}_y$ (W): Net annual average heat transfer to the ground, counted positively for heat rejection to the ground[4]
R_{10y} (m2.K/W): Effective thermal resistance of the ground computed with a 10-year heat pulse
$\dot{Q}_m$ (W): Net monthly average heat transfer to the ground
R_{1m} (m.K/W): Effective thermal resistance of the ground computed with a 1-month heat pulse
$\dot{Q}_h$ (W): Net 6-hour average heat transfer to the ground
R_b (m.K/W): Borehole overall thermal resistance
$F_{sc} = 0.04$ (-): Correction factor for short-circuit heat losses between the upward and downward flowing legs
R_{6h} (m.K/W): Effective thermal resistance of the ground computed with a 6-hour heat pulse
T_g (C): Undisturbed temperature of the ground
T_p (C): Ground temperature penalty
T_{Ent} (C): Temperature of the liquid entering the borefield
T_{Lvg} (C): Temperature of the liquid leaving the borefield

The effective resistances of the ground are computed according to the cylindrical heat source formulation from Carslaw and Jaeger (1947) considering a borehole diameter of 150 mm, a soil conductivity, specific heat capacity, and density of 2.3 W/m.K, 1000 J/kg.K, and 2600 kg/m3, respectively. This gives: $R_{10y} = 0.17, R_{1m} = 0.15, R_{6h} = 0.08$ m.K/W. The overall resistance of the borehole is computed based on the method from Kavanaugh and Rafferty (2014) considering DN40 DR11 HDPE pipes in a double-U configuration and a grout material with a conductivity of 2.0 W/m.K. This gives: $Rb = 0.06$ m.K/W. The hourly load data used for sizing are generated as described in §5.1.1, considering a chiller efficiency of $COP_{Cooling} = 7.0$ in cooling mode (with a condenser entering temperature of 18°C and an evaporator leaving temperature of 7°C) and $COP_{Heating} = 4.0$ in heating mode (with an evaporator entering temperature of 7°C and a condenser leaving temperature of 50°C). This gives the heat flow rate transferred to the main network as presented in Figure 2.

[4]This is the opposite convention as the one used in Kavanaugh and Rafferty (2014), and Equation 1 is rearranged accordingly.

The sizing rationale is then as follows. Starting from an undisturbed ground temperature of $T_g = 10°C$, the dominating heat rejection will enable reaching an equilibrium temperature of $T_g + T_p = 12.0°C$, which lies roughly in the middle of the target loop temperature range of $[9, 16]$ (C). From there, the auxiliary cooling system is designed to balance the heat transferred to the main loop on an annual basis, so $Q_y = 0$ is considered to size the borefield. The effect of the auxiliary cooling system on $\dot{Q}_m$ and $\dot{Q}_h$, i.e., near cooling design conditions, is neglected as explained in §4.3.4. This gives the following number of boreholes considering a borehole depth of 180 m.

$$\begin{aligned} n_{Heating} &= 705 \\ n_{Cooling} &= 1426 \end{aligned} \tag{2}$$

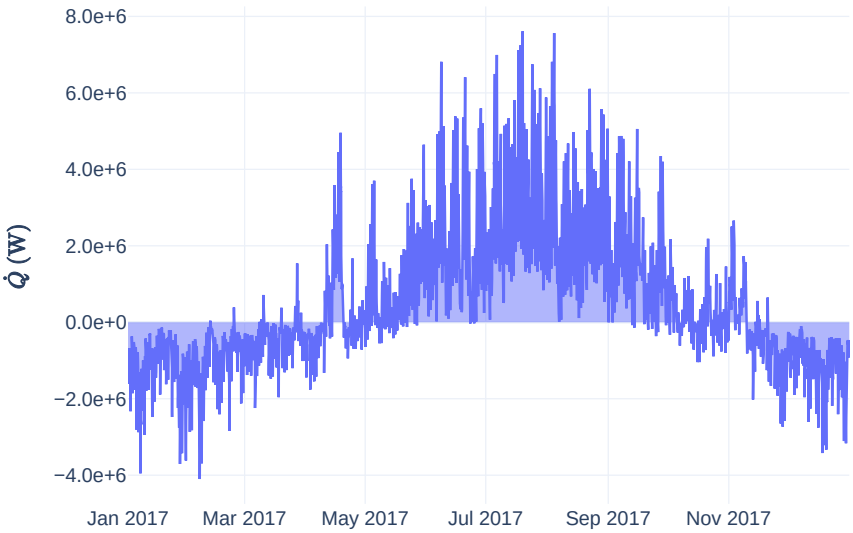

Figure 2: Hourly heat flow rate transferred to the main network (computed from EnergyPlus load data, see §5.1.1).

4.3.4. Auxiliary Cooling System

The selection of the auxiliary cooling system can be informed by the weather data statistics (see Figure 4) and the contribution of the different heat pulses to the sizing of the borefield based on Equation 1 (see Figure 3).

If cooling towers or dry coolers[5] are used, they will mainly be off during the hottest months considering the target loop supply temperature of 16°C. The auxiliary cooling system will be primarily used during the shoulder seasons to cool down the ground surrounding the borefield,

[5]Open cooling towers allow approaching the wet bulb temperature up to 2-4 K but require an intermediary heat exchanger to prevent an elevated oxygen concentration in the district loop. They can be operated even at low ambient temperature, under freezing conditions.

Dry coolers allow approaching the dry bulb temperature up to 3-4 K and can be directly connected to the district loop. To avoid the addition of glycol, they shall be enabled only if the ambient temperature is above 0°C.

and balance the heat transferred to the main loop on an annual basis. Considering the annual component from Figure 3, the impact on the size of the borefield is limited to about 10%. Therefore, if the supply temperature must be kept under 16°C to allow WSE cooling, the highest number of boreholes $n_{Cooling}$ is likely required. This will be verified by modeling auxiliary dry coolers (the benefits of an evaporative system are little in shoulder season operation) that are sized and controlled to balance the heat transferred to the main loop on an annual basis. Here, a whole-year simulation of the coupled system is needed for a proper sizing. The control sequence is as follows. The system is enabled based on a similar logic as the one implemented for the waterside economizer, see §4.1: a predicted leaving water temperature is computed at maximum and minimum fan speed, and the system is enabled if the temperature at maximum fan speed is lower than the entering temperature (considering a 1 K margin), and if the temperature at minimum fan speed is higher than the minimum supply temperature set point, and if the ambient temperature is above 0°C. When enabled, the fan speed is modulated between its minimum when the entering water temperature equals to the minimum supply temperature set point (considering a 1 K margin) and its maximum when the entering water temperature equals to the target equilibrium temperature of 12°C, see §4.3.3. The system is disabled if the actual leaving water temperature is higher than the entering water temperature, or if it is lower than the minimum supply temperature set point.

An alternative hybrid design option relies on auxiliary chillers, that can effectively contribute to lowering the heat rejection demand during the hottest months. In that case, the borefield can likely be downsized to the lowest number of boreholes $n_{Heating}$. An additional simulation experiment will be carried out to assess to what extent and with what control strategy such a configuration can provide compressor-less cooling capacity during an extreme week, i.e., keep the supply temperature of the loop under 16°C during the whole week without enabling the chillers. This configuration is not exclusive from the previous one, and dry coolers may be used as condenser water coolers, with a waterside economizer option to directly cool down the main loop at low ambient temperature.

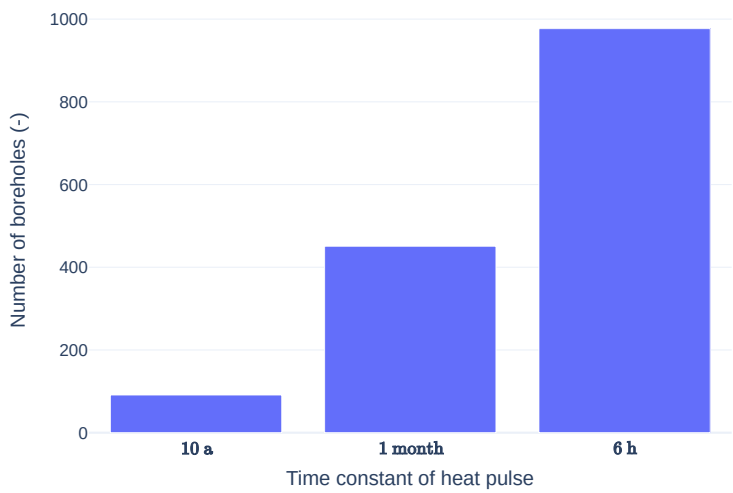

Figure 3: Contribution of the different heat pulses to the sizing of the borefield based on Equation 1 (including the yearly average not considered if compensated by an auxiliary cooling system).

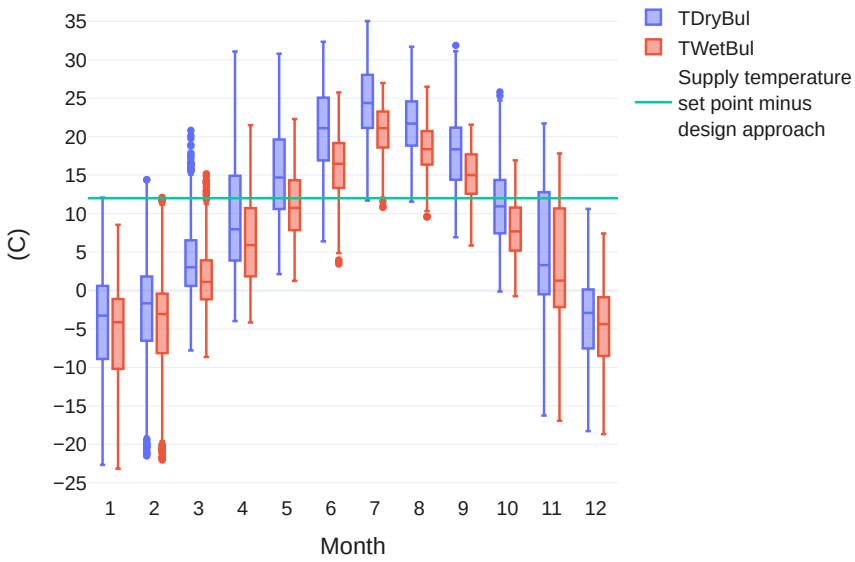

Figure 4: Monthly box plots of the hourly dry bulb and wet bulb temperature from a typical meteorological year (TMY3) in Chicago, IL.

5. Application to a Resilient Operating Mode

5.1. Description of the Simulation Experiment

5.1.1. Building Models

The original building models are taken from the US DOE commercial reference buildings database and represent new constructions (year 2004) of a medium office, a mid-rise apartment, and a hospital in Chicago IL, USA. The study focuses on the office building type where resilience metrics are computed based on proxy variables for thermal comfort. The other building types are included to model the load diversity of a typical mixed-use development project. A multiplier factor of 10 is applied to the office and apartment types to represent a cluster of similar buildings. The building models are used in two different ways.

First, simulating those models with EnergyPlus provides heating and cooling load data—the domestic hot water (DHW) loads are not considered in this study—which are used to size the systems. The resulting building loads are presented Figure 5, the total peak cooling and heating loads are 3.5 and 3.2 MW, respectively, and the annual energy is 8.9 and 5.8 GWh/y, for a total conditioned floor area of $103,590$ m2. For the apartment and hospital types, the corresponding time series are then directly used as inputs to the model of the DHC system. Here, the boundary of the Modelica model is the load side of the ETS component where the building loads are converted into a mass flow rate and temperature variation with an interface component approximating the emission/flow rate characteristic of the building HVAC system.

Second, for the office type, the EnergyPlus input data file is consumed to generate an FMU for Model Exchange that can be coupled to a Modelica model using the Spawn of EnergyPlus toolchain Wetter et al. (2020). Here, the boundary of the Modelica model encompasses the building HVAC system as well as the air volume of the rooms, while the building envelope is modeled with EnergyPlus. The building HVAC system is a variable air volume (VAV) system with hot water

reheat. The system components are sized based on the peak loads computed with EnergyPlus (with a cooling load diversity factor of 0.7) and the requirements from ANSI/ASHRAE 62.1-2019 (2019) for ventilation parameters and from ANSI/ASHRAE/IES 90.1-2019 (2019) for other limiting operating conditions. The control sequence is adapted from ASHRAE (2006). The main features of the implementation are described in Wetter et al. (2022), and some refactoring was carried out mainly for scalability (with 15 conditioned zones plus 3 plenum zones where the air return inlets are located) and to expose all sizing parameters in a central parameter record. However, some limitations from the original model pertain and call for caution and consolidation efforts for large multi-zone applications, namely: the model represents a single supply fan system with no return fan; the parametrization of the duct network is representative of a non-ducted return systems; there is no space static pressure control (unrealistic pressure values are indeed observed at high flow rate and low exhaust damper opening); the fan and motor efficiency is constant.

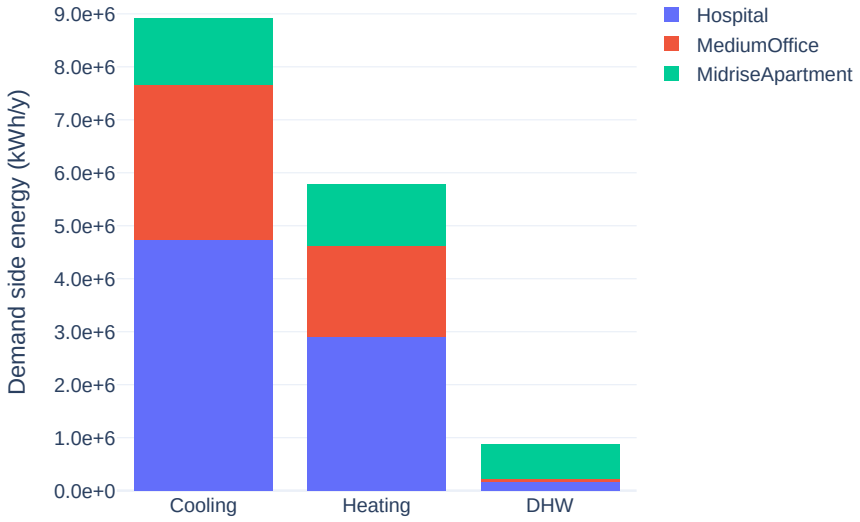

Figure 5: Building loads computed with EnergyPlus, integrated over the year, including the multiplier factors used to represent clusters of similar buildings (DHW loads are presented for reference but are not considered in this study).

5.1.2. Resilience Scenario and Metrics

Weather Data. The weather data for annual simulation is a typical meteorological year (TMY3) for Chicago, IL, USA. A so-called "resilience design day" is generated based on the most severe conditions in July from that TMY3 weather file, which happen to be more conservative than a design day generated based on the method proposed in ASHRAE (2017) Chapter 14 considering the annual 0.4% design dry-bulb temperature and the mean coincident wet-bulb temperature. During the resilience design day the dry-bulb temperature range is $[23.3, 35.0]$ (C), the wet-bulb temperature range is $[22.5, 26.9]$ (C), and the global horizontal irradiance peaks at 931 W/m2. The resilience design day is repeated 7 times during the month of July to generate a "resilience design week" over which the comfort analysis is performed.

Internal Heat Gains. The nominal heat gains from the original EnergyPlus input data file are corrected to account for an adaptive scenario[6] during the extreme week where the office building operates on backup power. The nominal number of people and plug power is reduced by 30%, the nominal lighting power is reduced by 70%, and no heat gains from the elevators and domestic hot water system are considered.

Resilience Metrics. The key metrics and the methodology to gauge the resilience of the office building during the extreme week are taken from Mathew et al. (2021). The number of degree-hours beyond a tolerability threshold (30°C) is first computed for each thermal zone[7]. The referenced study then considers that the zone cannot be occupied if that number exceeds 34 K.h per day while the temperature is still beyond tolerable. This contributes to increasing a so-called number of occupant hours lost (OHL) by the nominal number of people in the zone. This never happens in our case study, i.e., the number of OHL is always zero for all thermal zones. For that reason, our analysis is only based on the number of degree-hours above tolerable. In addition, we only consider typical operating hours from 7am to 7pm, from Monday to Friday.

5.2. Results

This section first presents the analysis of the indoor environmental quality (IEQ) that can be achieved during the extreme week considering the district loop target temperature range of $[9, 16]$ (C) and the sensitivity to various sizing parameters of the building HVAC system. We will then discuss the characteristics and sizing of the central components of the DHC system that are required to maintain the supply temperature within that temperature range.

5.2.1. Indoor Environmental Quality in a Compressor-Less Operating Mode

Disabling the chillers and relying only on WSE cooling during the extreme week with a service supply temperature of 16°C does not yield any occupant hours lost in the office building. The evolution of the operative temperature is provided Figure 6, together with the power drawn by the fans, pumps and chillers, and the total cooling heat flow rate. The case with WSE cooling is compared with the base case with chiller cooling. The WSE mode yields a reduction of about 60% in the total power at the peak, while still meeting 70% of the load. This is achieved despite a high chiller COP close to 7 in the base case. The significant fan power results from sizing the system air flow rate based on the peak loads and a design coil leaving air temperature of 13°C, with a diversity factor of 70%. This leads to a design air flow rate of 44478 m3/h, and an air change rate ranging from 3 to 9 h-1 among the conditioned zones. Downsizing the system air flow rate by means of a lower design coil leaving air temperature would be beneficial to the fan power but detrimental to the IEQ in the WSE cooling mode, where the cooling coil valve is fully open and the supply air temperature is free-floating. During the operating hours the average building HVAC system COP (accounting for the AHU fan, the primary and secondary pumps, and the chiller) is equal to 5.2 in the case of chiller cooling and 7.3 in the case of WSE cooling, i.e., an increase of 40% in the system efficiency due the WSE mode.

The number of degree-hours above tolerable is presented Figure 7 for each of the 15 thermal zones. Without oversizing the cooling coil (i.e., with a sizing coefficient of 1.0), the number of

[6] This assumption differs from Mathew et al. (2021) where only the loss of the HVAC system is considered without any concomitant reduction in the internal heat gains.

[7] For the sake of simplicity, we use here the operative temperature, as opposed to the standard effective temperature in Mathew et al. (2021).

degree-hours is below 6 K.h in the limiting zone during the limiting day[8], while the median value remains equal to zero, meaning that a tolerable IEQ can be achieved in a low-power mode in the majority of the thermal zones.

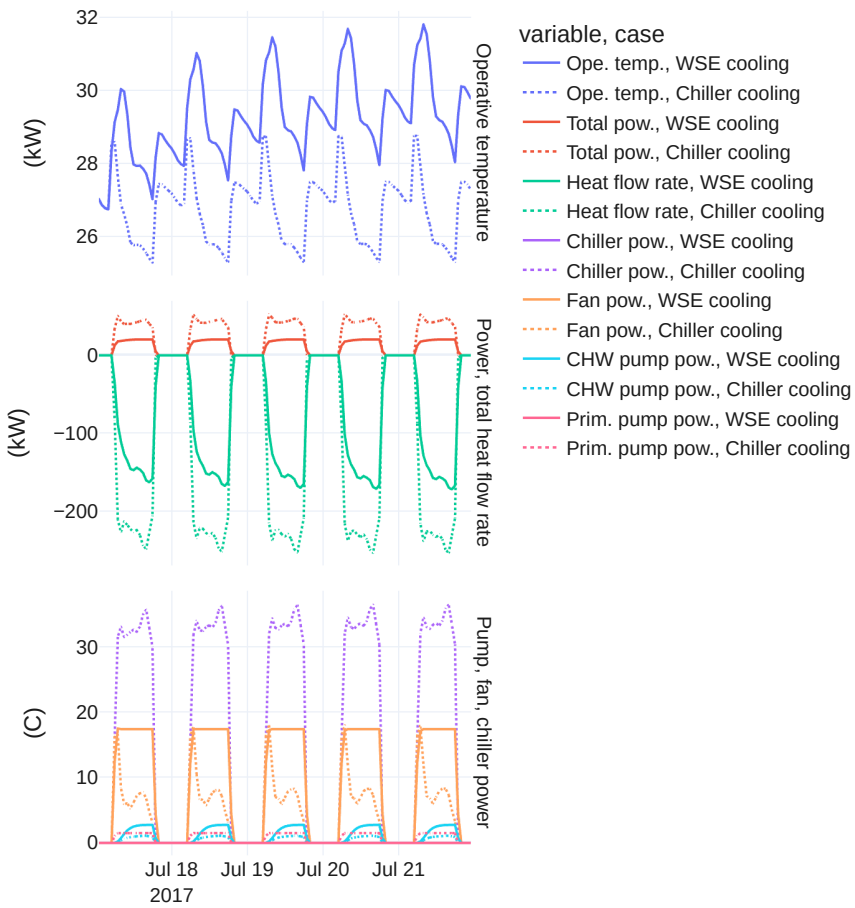

Figure 6: Operative temperature in the limiting zone; total power and cooling heat flow rate; chiller, pump and fan power – WSE cooling compared to chiller cooling during the extreme week.

Cooling Coil Sizing. The sensitivity to the cooling coil capacity is analyzed by applying a multiplier factor to the design UA-value of the coil model, considering that the design pressure drop is increased by the same factor for both the air and the chilled water side. The CHW pump design flow rate is considered identical in all cases. Our premise is that the integration into an existing system can be made without modifying the CHW distribution pump, provided that sizing margins are available on the pump operating point at maximum speed (which is typically the case).

As illustrated in Figure 7, oversizing the coil by a factor 1.6 reduces the number of degree-hours above tolerable by a factor 2 for the limiting zone, while the average power during the operating

[8]Mathew et al. (2021) suggests a limit of 34 K.h per day to decide that a zone cannot be occupied and to start incrementing the thermal OHL count.

hours is increased by about 30% and the total cooling heat flow rate is increased by less than 15%, which corresponds to a diminution in the system COP from 7.3 to 6.4.

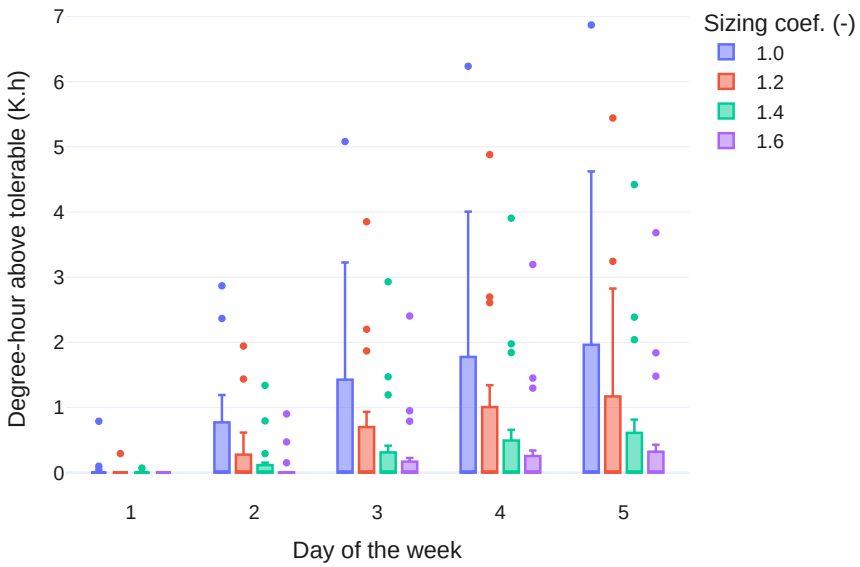

Figure 7: Sensitivity to the cooling coil sizing – Daily box plots of degree-hours above tolerable as distributed over all thermal zones.

Fan Sizing. The sensitivity to the fan sizing is analyzed by applying a multiplier factor k to the nominal volume flow rate and k^2 to the nominal head of the fan. The flow resistance of the duct network and all other AHU components is considered identical in all cases. Our premise is that the integration into an existing system can be made by only changing the AHU fan.

As illustrated in Figure 8, oversizing the fan has a limited impact on the number of degree-hours above tolerable. Beyond a 20% oversizing factor, the impact is even detrimental. This is because the power drawn by the fan motor scales cubic with the sizing factor, and so does the dissipated heat flow rate. This leads to an increase in the supply air temperature that is no more compensated by the increased air flow rate. Comparing the base case (sizing factor equal to 1.0) with the optimum case (sizing factor equal to 1.2), the average power during the operating hours is increased by about 60% while the total cooling heat flow rate is increased by less than 10%, which corresponds to a diminution in the system COP from 7.3 to 4.8. The latter value indicates that the WSE cooling mode is then less efficient than the chiller cooling mode.

The conclusion is entirely different when oversizing the whole air system, with the duct network oversized to keep the same pressure drop per length at design flow rate. This if illustrated Figure 9 where the sizing coefficient of 1.4 corresponds to no load diversity accounted for when sizing the system (as opposed to a 70% load diversity factor used in the base case). The degree hours above tolerable get canceled out for all thermal zones, with an average system COP only reduced from 7.3 to 6.8.

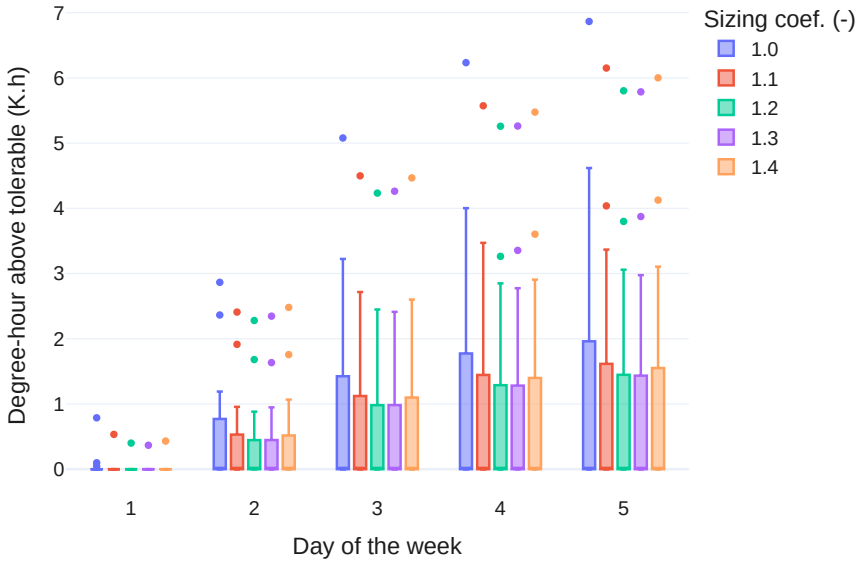

Figure 8: Sensitivity to the fan sizing – Daily box plots of degree-hours above tolerable as distributed over all thermal zones.

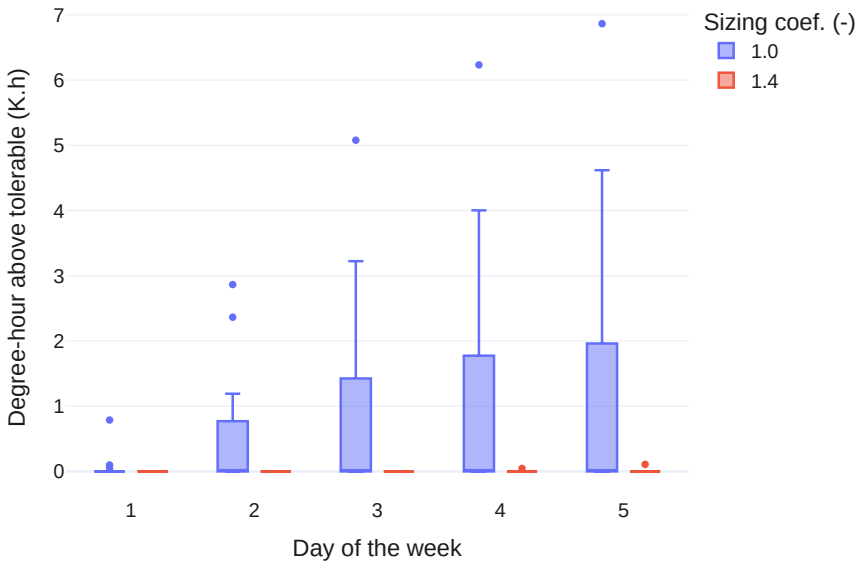

Figure 9: Sensitivity to the air system sizing – Daily box plots of degree-hours above tolerable as distributed over all thermal zones.

5.2.2. DHC Central Components

Geothermal Borefield and Dry Coolers. The sensitivity to the size of the borefield is illustrated Figure 10 and Figure 11 by plotting the supply temperature and the transferred energy as computed by simulating five years of operation for different numbers of boreholes within the range given by Equation 2. Figure 11 shows that the energy transferred to the ground is closed to balanced on an annual basis and that the five year horizon can be used to analyze the operation. We verify that the initial sizing based on Equation 1 is valid for that hybrid system with auxiliary dry coolers, and that the maximum number of boreholes is indeed required to maintain the supply temperature below 16°C. The corresponding sizing ratio is 75 m/kW (total length of boreholes divided by the system capacity) which lies far outside the range of $[10, 30]$ (m/kW) observed on conventional systems (Kavanaugh and Rafferty, 2014). This is explained by the low temperature approach of about 6 K that is required here for the ground heat exchanger, as opposed to the range of $[10, 25]$ (C) generally used for conventional geothermal systems without any requirement for compressor-less cooling. This yields a first cost of the geothermal system that is likely prohibitive and calls for exploring a hybrid design with a lower number of boreholes and auxiliary chillers. Figure 11 also shows transient temperature variations below the limit of 9°C. Those are due to the timers used in the control sequence for the dry coolers and could be eliminated, although this does not impact our analysis. This is illustrated Figure 12 where the temperature is provided at the borefield outlet and at the cooling plant outlet (district supply) for the case with the maximum number of boreholes. The dry coolers are effectively cooling the loop in the shoulder seasons, but also partly in the cold season where the system is heating dominated (see Figure 5) and would benefit from a higher supply temperature, which could be achieved by an integration of the dry coolers upstream the borefield.

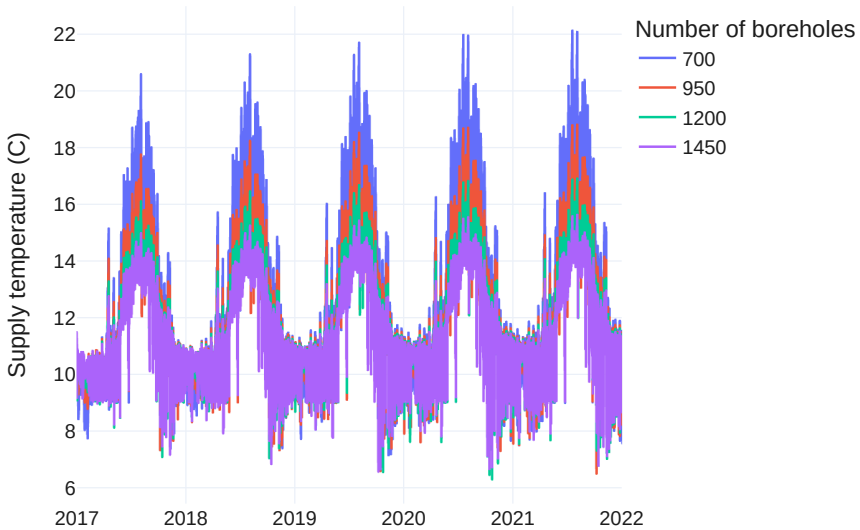

Figure 10: Sensitivity to the geothermal borefield sizing, case with central dry coolers - District water supply temperature.

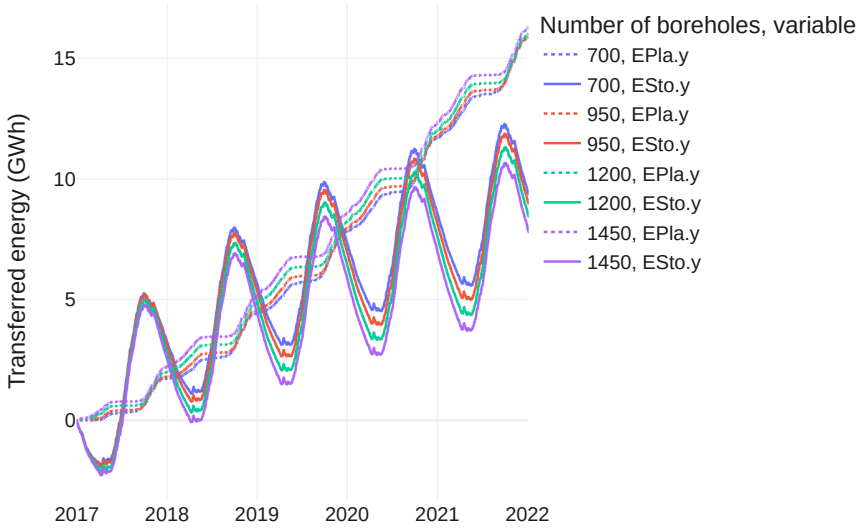

Figure 11: Sensitivity to the geothermal borefield sizing, case with central dry coolers - Energy transferred from the district loop through the borefield ($ESto.y$) and through the dry coolers ($EPla.y$).

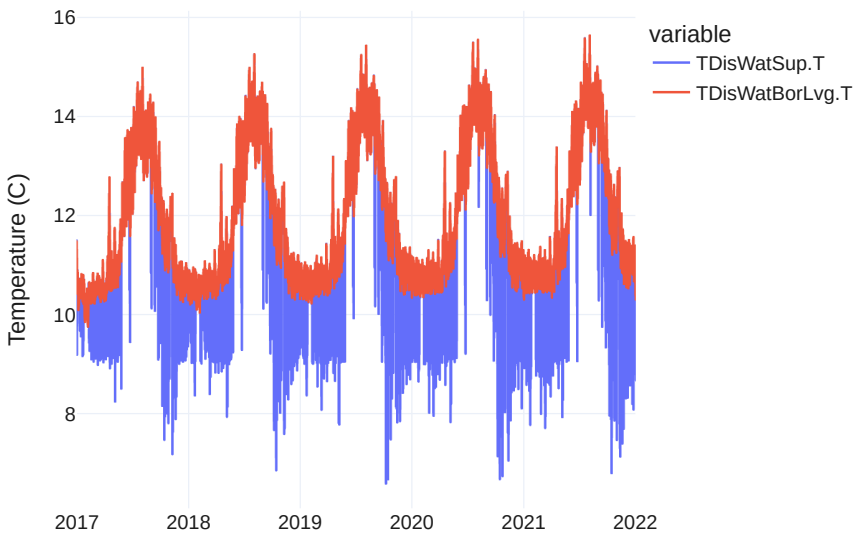

Figure 12: Illustration of the dry coolers operation on the case with 1450 boreholes - District water supply temperature ($TDisWatSup.T$) and borefield leaving temperature ($TDisWatBorLvg.T$).

Geothermal Borefield and Central Chiller Plant. Using air cooled chillers as the auxiliary cooling system instead of the dry coolers gives the supply temperature trajectory shown in Figure 13, focusing on a single year of operation close to the equilibrium state of the system. In this configuration, both the central chillers and the distributed chillers are disabled in WSE cooling mode so that the cooling function only relies on the ground heat exchanger during the extreme week. In chiller cooling mode, the central plant is controlled to track the maximum supply temperature set point.

We can observe that the central chillers do not help reduce the number of installed boreholes and that the maximum size of the borefield is still required to maintain the supply temperature set point during the extreme week. The fact that the supply temperature is higher on an average than in the case with the dry coolers shows that the chiller plant is less capable of precooling the surrounding ground when simply controlled based on the supply temperature set point, and that an advanced control strategy would be needed to better leverage the cooling capacity of the plant.

As an simple control alternative, the temperature set point of the plant is reduced to 11°C in the configuration with the smallest borefield size, i.e., the highest temperature approach for the ground heat exchanger. This configuration is close to meet the temperature requirement during the extreme, however, it exhibits a significant temperature drop below the minimum set point. This behavior is not the effect of a control transient as in the case with the dry coolers, but rather the consequence of a lowest amount of heat stored in the ground over the cooling dominated period—part of it being released into the atmosphere by the central cooling plant. This reveals the need for additional seasonal heat storage capacity.

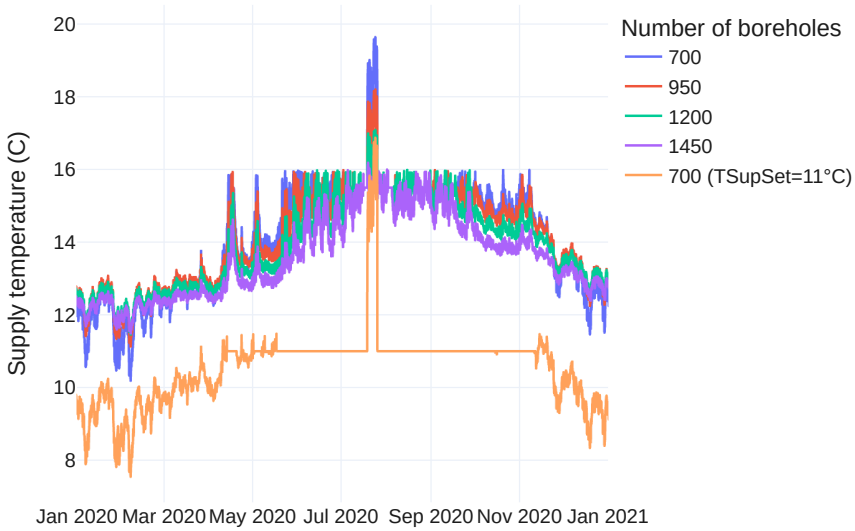

Figure 13: Sensitivity to the geothermal borefield sizing, case with central chillers - District water supply temperature.

5.2.3. Power and Energy Analysis

Waterside Economizer

6. Conclusion

We considered an all-air system as it is the most widely used in the US and the least favorable for high-temperature cooling (as opposed to radiant cooling systems for instance). This help demonstrate how novel DHC technologies can be deployed to existing buildings and that compressor-less cooling opportunities are accessible to typical air-based systems, providing proper sizing adjustments.

Future studies should investigate the benefits of source-side to source-side connection (indirect heat recovery at lower lift) as opposed to direct heat recovery at higher lift.

7. Acknowledgements

This work was supported by the Laboratory Directed Research and Development Program of Lawrence Berkeley National Laboratory under U.S. Department of Energy Contract No. DE-AC02-05CH11231.

Most of the component models that this work relies on were developed in projects supported by the Advanced Manufacturing Office and the Building Technologies Office of the U.S. Department of Energy, under the same contract number.

Appendix A. Modeling Hydronic Systems

When integrating the ETS model into the whole DHC system model, significant effects of hydronic imbalance were first observed, with the remote ETSs being starved and unable to meet the supply temperature set point, and the ETSs closer to the pump operating at higher flow rates than design. In addition, convergence issues of the Newton solver appeared, mainly related to the waterside economizer operation.

The first effect was certainly expected using a pressure-driven model of the hydronic system, with no specific care for balancing the connected units. However, and as in real systems, that effect was not expected to disturb the operation to the extent that was observed. Indeed, a controller—controlling for instance a supply temperature or a temperature difference—should limit the primary flow rate under the design values (provided that the primary fluid temperature remains close to the design value). In addition, the heat emission characteristic is supposed to limit the impact of flow shortage, with 50% of the design mass flow rate still providing about 90% of the design heat flow rate for a heat exchanger with 10 K primary temperature range at design. The only disturbing effects that were expected, and indeed observed, pertain to the low valve authority of the primary control valves that causes control issues, and to the pump speed which is often maxed-out due to the inability to maintain the pressure drop at the remote ETS.

The reason why the ETSs close to the pump often operate at a higher flow rate than design is related to the control based on the heat or cold rejection demand (see §4.1) that first opens the primary control valve (up to its full opening), then resets down the CHW supply temperature. So the ETSs that are exposed to a higher pressure drop than the design value use the excess flow rate instead of resetting the supply temperature to increase the temperature difference (or rate of heat transfer) with the primary side of the heat exchanger.

Regarding the numerical issues that were encountered we must acknowledge the challenges that remain when modeling closed loop hydronic systems (typically with feedback of a remote differential pressure sensor or of the valve positions to control the main distribution pump). There has been extensive work that was already carried out to formulate actuator models limiting the size of the DAE systems and exhibiting the proper smoothness required by Newton solvers (Jorissen et al., 2015). Namely, each actuator model of the Modelica Buildings Library offers the option to solve either for the mass flow rate or for the pressure drop, which breaks the algebraic loop created when two actuators are in parallel or in series, respectively. In addition they provide the option for an additional state variable (mimicking the actuator motion delay) which is another means to avoid an algebraic loop. In our case, those two modeling features did not solve the convergence issues.

The resolution came from integrating a pressure independent control valve (PICV) into the ETS model to modulate the mass flow rate of the service water through the heat exchangers. To represent the various technologies of PICVs (dynamic balancing valve in series with a control valve, or built-in flow meter and controller) the model idealizes the physics by solving the simple equation $\dot{m}_{Act} = u * \dot{m}_{Nom}$, where u is the control signal and $\dot{m}_{Act}$ and $\dot{m}_{Nom}$ are the actual and design mass flow rate, respectively. The complexity of the model lies in the requirement to properly represent the valve limiting flow characteristics (leakage and full opening) and to compute a pressure drop and a mass flow rate that are continuously differentiable while transitioning between the two characteristics (which is a requirement to apply Newton solvers). Using that valve model to modulate the service water flow rate offers key benefits, similar to the ones obtained by the use of PICVs in real hydronic systems.

1. The system is dynamically balanced. The primary flow rate can only marginally exceed the design value. Furthermore, this holds true for any operating point, and any location in the distribution network. To the contrary, balancing valves that are commissioned at design conditions may lead to low pressure differences at the boundaries of the control valves close to the distribution pump in the case of closed loop control based on a remote pressure drop sensor and with low demand on the remote valves.
2. The controllability is optimal. The relationship between the control signal (varying between 0 and 1) and the mass flow rate (varying between close to 0 and close to the design value) is indeed close to linear. To the contrary, with standard control valves, a potentially large range of flow rate variation (spanning beyond the design value) may be mapped to a limited range of variation of the control signal (depending on the valve authority), leading to tedious controller tuning or control instabilities.

In addition, the simulation model is simplified due to the ideal model of the flow rate control loop, for instance when modeling a waterside economizer where the primary valve position is actuated so that the primary mass flow rate equals the chilled water mass flow rate. This eliminates the need for a controller (and for tuning), while reducing the number of state variables and therefore the time to solution, especially for such control loops with fast pressure-driven dynamics.

References

AFPG, 2020. La boucle d'eau tempérée à énergie géothermique. Technical Report 01/ RGEOTBE01 XM-HL-JMP. AFPG. Paris, France. URL: http://www.afpg.asso.fr/wp-content/uploads/2020/05/APFG_GUIDE_BoucleEau_BAT3.pdf.

ANSI/ASHRAE 62.1-2019, 2019. Ventilation for Acceptable Indoor Air Quality. Standard. ASHRAE. Atlanta, GA.

ANSI/ASHRAE/IES 90.1-2019, 2019. Energy Standard for Buildings Except Low-Rise Residential Buildings. Standard. ASHRAE. Atlanta, GA.

ASHRAE, 2006. Sequences of Operation for Common HVAC Systems. ASHRAE. Atlanta, GA.

ASHRAE, 2017. Fundamentals. ASHRAE. Atlanta, GA.

Buffa, S., Cozzini, M., D'Antoni, M., Baratieri, M., Fedrizzi, R., 2019. 5th generation district heating and cooling systems: A review of existing cases in europe. Renewable and Sustainable Energy Reviews 104, 504–522. doi:10.1016/j.rser.2018.12.059.

Buffa, S., Soppelsa, A., Pipiciello, M., Henze, G., Fedrizzi, R., 2020. Fifth-generation district heating and cooling substations: Demand response with artificial neural network-based model predictive control. Energies 13. doi:10.3390/en13174339.

Carslaw, H., Jaeger, J., 1947. Conduction of Heat in Solids, Oxford: Claremore Press.

Cline, L., Bakkum, B., 2020. Applications Engineering Manual – Central Geothermal Systems. TRANE. SYS-APM009C-EN.

Jorissen, F., Wetter, M., Helsen, L., 2015. Simulation speed analysis and improvements of modelica models for building energy simulation, in: The 11th International Modelica Conference, Versailles, France. doi:10.3384/ecp1511859.

Kavanaugh, S., Rafferty, K., 2014. Geothermal Heating and Cooling – Design of Ground-Source Heat Pump Systems. ASHRAE. Atlanta, GA. RP-1674.

Mathew, P., Sanchez, L., Lee, S.H., Walter, T., 2021. Assessing the energy resilience of office buildings: Development and testing of a simplified metric for real estate stakeholders. Buildings 11. doi:10.3390/buildings11030096.

Mattsson, S.E., Elmqvist, H., 1997. Modelica – An international effort to design the next generation modeling language, in: Boullart, L., Loccufier, M., Mattsson, S.E. (Eds.), 7th IFAC Symposium on Computer Aided Control Systems Design, Gent, Belgium. pp. 1–5. URL: http://www.modelica.org/publications/papers/CACSD97Modelica.pdf.

Sommer, T., Sulzer, M., Wetter, M., Sotnikov, A., Mennel, S., Stettler, C., 2020. The reservoir network: A new network topology for district heating and cooling. Energy 199, 117418. doi:10.1016/j.energy.2020.117418.

Sulzer, M., Werner, S., Mennel, S., Wetter, M., 2021. Vocabulary for the fourth generation of district heating and cooling. Smart Energy 1, 100003. doi:10.1016/j.segy.2021.100003.

Taylor Engineering LLP, Taylor, S.T., Gill, B., Kiriu, R., 2019. Advanced Sequences of Operation for HVAC Systems – Phase II Central Plants and Hydronic Systems. Technical Report Research Project 1711. Task 5: Reporting of Findings. ASHRAE. Atlanta, GA.

Wetter, M., Benne, K., Gautier, A., Nouidui, T.S., Ramle, A., Roth, A., Tummescheit, H., Mentzer, S., Winther, C., 2020. Lifting the garage door on spawn, an open-source bem-controls engine, in: Proc. of Building Performance Modeling Conference and SimBuild, Chicago, IL, USA. URL: `https://simulationresearch.lbl.gov/wetter/download/2020-simBuild-spawn.pdf`.

Wetter, M., Ehrlich, P., Gautier, A., Grahovac, M., Haves, P., Hu, J., Prakash, A., Robin, D., Zhang, K., 2022. OpenBuildingControl: Digitizing the control delivery from building energy modeling to specification, implementation and formal verification. Energy 238. doi:`10.1016/j.energy.2021.121501`.

Wetter, M., Fuchs, M., Grozman, P., Helsen, L., Jorissen, F., Lauster, M., Mueller, D., Nytsch-Geusen, C., Picard, D., Thorade, M., 2015. IEA EBC Annex 60 Modelica Library - an international collaboration to develop a free open-source model library for buildings and community energy systems, in: The 14th International Modelica Conference, p. 395–402.

Wetter, M., Hu, J., 2019a. Quayside Energy System Analysis. Technical Report LBNL-2001197. Lawrence Berkeley National Laboratory. Berkeley, CA. URL: `https://simulationresearch.lbl.gov/wetter/download/LBNL-2001197.pdf`.

Wetter, M., Hu, J., 2019b. Quayside Energy Systems Analysis. Technical Report. Lawrence Berkeley National Laboratory. Berkeley, CA.

Wetter, M., van Treeck, C., Helsen, L., Maccarini, A., Saelens, D., Robinson, D., Schweiger, G., 2019. IBPSA Project 1: BIM/GIS and Modelica framework for building and community energy system design and operation – ongoing developments, lessons learned and challenges, in: IOP Conference Series: Earth and Environmental Science 323.